(International Print/Online Journal)

SJIF IMPACT FACTOR: 5.565
PUBMED-National Library of Medicine ID-101739732

ISSN (Print): 2209-2870
ISSN (Online): 2209-2862

International Journal of Medical Science and Current Research (IJMSCR)
Available online at: www.ijmscr.com
Volume3, Issue 4, Page No: 372-389
July-August 2020

Variation Natures of Brain Tumour before and After COVID-19

[1]Shawni Dutta and [2]Prof. Samir Kumar Bandyopadhyay

[1]Department of Computer Science, [2] Academic Advisor

The Bhawanipur Education Society College, Kolkata, India

***Corresponding Author:**
Prof. Samir Kumar Bandyopadhyay
Academic Advisor, The Bhawanipur Education Society College, Kolkata, India

Type of Publication: Original Research Paper
Conflicts of Interest: Nil

ABSTRACT

Life threatening diseases in both male and female are Brain tumor, stroke, hemorrhage and multiple sclerosis (MS). The most common and widespread disease among these brain diseases is Brain tumor. Early and accurate diagnosis of brain lesion is vital for determining accurate treatment and prognosis. However, the diagnosis is a very challenging task and can only be performed by specialists in neuroradiology. A dataset of 30678 patients are collected from Government Hospitals and Private Hospitals in West Bengal before COVID-19 and after COVID-19. The classification of patients is based on three classes- Normal, Sign of Tumor and Presence of Tumor. The reports of MRIs of patients in January 2020 and February 2020 are collected from different hospitals. It is treated as dataset before COVID-19. Reports of MRIs of patients in April 2020, May 2020 and June 2020 are dataset during COVID-19. The entire datasets are accumulated for testing of any change in patients MRIs after the official announcement of new virus COVID-19 in March 2020. The aim of the paper is in two parts. The first part proposed a method for detection of five major types brain tumours. The second part is to make a comparison of any change in size of tumour in MRIs of patients before and after COVId-19. All collected MRIs reports are diagnosed by radiologists of hospitals.

Keywords: Brain Tumor, COVID-19, Glioma, Meningioma, Metastatic adenocarcinoma, Metastatic bronchogenic carcinoma, Sarcoma

INTRODUCTION

Brain tumors forms the second most cause for cancer related deaths in children and adults. A tumor can be graded in to several stages in accordance to the analysis of abnormality of the tumor cells and tissues. This grading gives us the acute probability of tumor growth in size and its spreading. Tumor grade can be determined using biopsy. It is to be noted that grading of tumor is not same as cancer stages. The accurate diagnosis of brain tumors types is sometimes very difficult due to its high complexity and there are large variations. Five major types of brain tumors: 1) Glioma, 2) Meningioma, 3) Metastatic adenocarcinoma, 4) Metastatic bronchogenic carcinoma, and 5) Sarcoma are considered for computerized classification [1]. A database has been created that contains images associated with its corresponding class label. Images from this database were used in testing and training the classifiers.

In the first stage MRI image is taken as input and is normalized. The second stage includes extraction of feature vectors from the image which results in reducing redundancy of data to serve as the input to the classifier. The classification stage classifies the important feature for detection of tumour [2].

The brain tumor diagnosis process during COVID-19 needs attention whether shape of the abnormality is detected or not. If there is any change in the size of tumour then it requires immediate attention for treatment [13-16].

A study over patients has been made to identify any changes in size of tumour before or after COVID-19. This paper also detects change of size of tumour.

Literature Review

The most important aim of brain MRI analysis is to extract clinical information that would improve diagnosis and treatment of disease. Extracting clinical information requires detection and segmentation of normal and abnormal tissues. In the recent days CAD system is used to enhance diagnostic capabilities of physicians and reduce the time required for accurate diagnosis [3].

Computer aided detection of brain tumors, stroke lesions, hemorrhage lesions, and multiple sclerosis lesions are the most difficult issues in field of abnormal tissues segmentations because of many challenges [4-5]. The brain injuries are of varied shapes and also distort other normal and healthy tissues structures. Intensity distribution of normal tissues is very complicated and there exist some overlaps between different types of tissues. Over the last decade various approaches have been proposed for the same. Some researcher work on segmentation problem through machine learning methods. It is meant a well trained model that can determine whether a pixel belongs to a normal or abnormal tissue. Brain tumors are one of the most common brain diseases, so detection and segmentation of brain tumors in MRI are important in medical diagnosis [6].

Supports Vector Machines (SVMs) are popular tools for classification by maximize the margin between classes of data that is independent and identically distributed. A SVM classification to classify the brain into the abnormal and normal classes using T1-weighted and contrast enhanced T1- weighted images [7]. This system used patient-specific training and compared classification of normal and abnormal using SVM classifier. It used the standard 2-class method and the more recent 1-class method [8]. The SVM method has the advantage of generalization and working in high dimensional feature space. It assumes that data are independently and identically distributed. Segmenting medical images with in-homogeneity and noise are creating problems of such classifiers.

Artificial neural network (ANN) is one of the powerful artificial intelligence techniques that have the capability to learn from a set of data and construct weight matrices to represent the learning patterns. Each node in an ANNs is capable of performing elementary computations [9]. Neural networks represent both linear and nonlinear relationships and have the ability to learn these relationships directly from the data. Traditional linear models are simply inadequate since it contains nonlinear characteristics [10]. Because of the many interconnections used in a neural network, spatial information can be easily incorporated into its classification procedures.

Neural networks execute very well on complicated, difficult, multivariate non-linear domains, such as tumour, stroke, and hemorrhage segmentation where it becomes more difficult to use decision trees, or rule-based systems. They also perform a little better on noisy fields and there is no need to assume a fundamental data allocation such as usually done in statistical modelling [11].

The care of brain tumour patients must be a main concern of European neuro-oncologists throughout the time of the pandemic. Data are still very sparse regarding Covid-19 in cancer patients in general [12]. Patients with brain tumours comprise a heterogeneous group with regard to age, symptom severity and prognosis. One should consider the best possible timing of surgery or oncological therapy. The risk to the patient increases if treatment is delayed.

Data Set

Dataset is a collection of similar and related data stored for processing. Further this can be defined as a collection of data that contains individual data units organized in a specific format. A data set generally contains a collection of a number of types of data. Medical dataset can be defined as a collection of pieces of information, especially those that are part of a collection to be used for the the diagnosis of diseases. In this paper data set, containing brain MRIs from from different Government hospitals as well as from Private Hospitals. Normally, hospitals

Volume 3, Issue 4; July-August 2020; Page No.372-389

stored the reports of patients MRIs prepared by radiologists. The hospitals provided all information for analysis due to the present scenario. The images are classified into normal, tends to be sign of tumour and also patients who already detected as brain cancer patients. These detections are based on the diagnosis of radiologists. The size of tumour is also classified according to the type of tumour present.

Proposed Method

The objective of the paper is to find out the presence of abnormal mass created in normal patients and as well as in tends to breast cancer patients. Also if there is any change of masses in confirmed brain cancer patients due to COVID-19 then it has to be specified for immediate treatment.

Tumour detected MRI of brain slices is selected for classification. Artifacts and skull elimination is used to remove unnecessary regions of MRI. Next these are normalized to a range for feature extraction process. In the classification step, the model is first trained using training dataset obtained from the image database which also defines the class labels being used. After performing the training on set of existing known data set then test the data for appropriate classes that help in correct medical decision making and diagnosis of brain tumour. The brief implementation of the technique has been shown in figure 1.

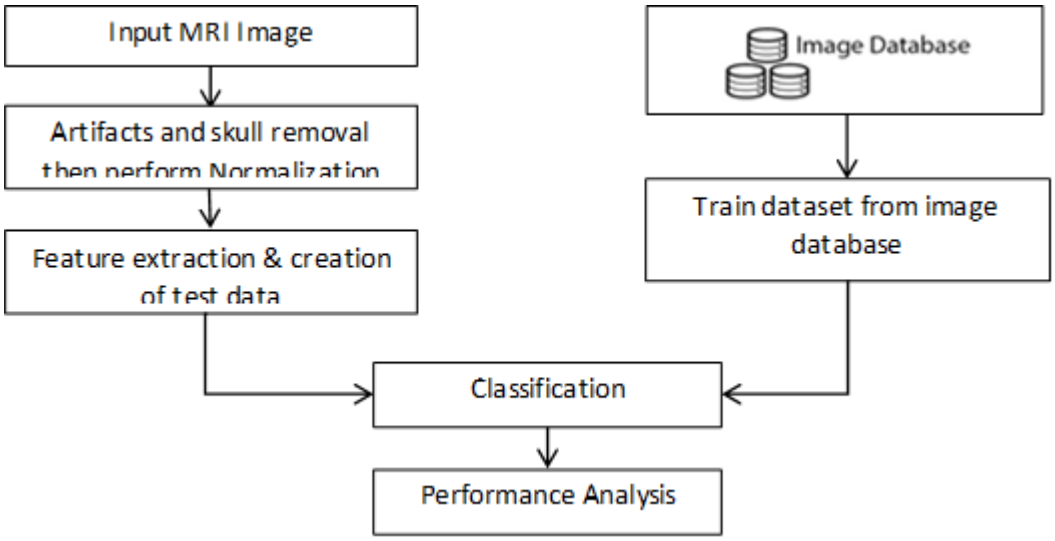

Figure 1: Workflow of the tumour classification

Features selection

Histogram of an image represents the concise statistical information contained in the image. Now consider that $f(x, y)$ is the function that represents the intensity level for each pixel (x, y) in the image, where $x = 1,2,\Lambda\ , A$ and $y = 1,2,\Lambda\ , B$. Grey-level histogram calculation involves each individual pixel. Probability density for each occurring pixel intensity level $0,1,\Lambda\ , N-1$ is calculated dividing them with $h(i)$ by total number of pixels. This can be represented as:

$$p(i) = \frac{h(i)}{AB} \quad for\ i = 0,1,\Lambda\ , N-1 \tag{1}$$

$$h(i) = \sum_{x=1}^{A}\sum_{y=1}^{B}\delta(f(x,y),i) \tag{2}$$

Volume 3, Issue 4; July-August 2020; Page No.372-389

Here $h(i)$ is the intensity level histogram function for the whole image and for each intensity level i. Here we have taken $\delta(i, j)$ as the kronecker delta function that can be given as:

$$\delta(i, j) = \begin{cases} 1, & i = j \\ 0, & i \neq j \end{cases} \quad (3)$$

Various useful parameters can be derived from the histogram to describe the statistical information about the image. These parameters are taken to be parameters for feature extraction. They are described below:

- *Mean:* The average value of intensity of the image and can be given as:

$$\mu = \sum_{i=0}^{N-1} i \cdot p(i) \quad (4)$$

- *Variance is defined as:*

$$\sigma^2 = \sum_{i=0}^{N-1} (i - \mu)^2 \, p(i) \quad (5)$$

- *Skewness:* Gives us the measure of the amount of symmetry of the histogram around mean. It can be given by:

$$\mu_3 = \sigma^{-3} \sum_{i=0}^{N-1} (i - \mu)^3 \, p(i) \quad (6)$$

- *Kurtosis:* Measures the flatness in the histogram and is given by:

$$\mu_4 = \sigma^{-4} \sum_{i=0}^{N-1} (i - \mu)^4 \, p(i) - 3 \quad (7)$$

- *Entropy:* Represents the uniformity of the histogram and is given by:

$$H = \sum_{i=0}^{N-1} p(i) \log_2[p(i)] \quad (8)$$

- *Energy:* Represents the mean of squared value of the pixel intensity and can be given as:

$$E = \sum_{i=0}^{N-1} [p(i)]^2 \quad (9)$$

All the mentioned parameters give us the information extracted from the local image histograms and can be used for texture segmentation. The normalization as given in previous step results in better texture discrimination accuracy. One of the major advantages of using these parameters is that they are simple, but they are not able to completely characterize texture. To solve this joint probability distributions of pixel pairs are required. Using this definition second order histogram known as grey-level co-occurrence matrix $h_{d\theta}(i, j)$ has been considered. The image matrix is divided by the total number of neighbouring pixels $R(d, \theta)$ in the image, the resulting image becomes the joint probability $p_{d\theta}(i, j)$ for two pixels with distance d between them and along the direction i and j. Value for $d = 1,2$ and $\theta = 0^o, 45^o, 90^o, 135^o$ are normally used. For a given image with intensity function $f(x, y)$ and

Volume 3, Issue 4; July-August 2020; Page No.372-389

N discrete intensity values, matrix $h_{d\theta}(i,j)$ and defining the parameters i and j as:

$$f(x_1, y_1) = i \quad \text{and} \quad f(x_2, y_2) = j \tag{10}$$

where $$(x_2, y_2) = (x_1, y_1) + (d\cos\theta, d\sin\theta) \tag{11}$$

This results in a matrix dimension equal to the number of intensity levels and for each distance d and orientation θ. Thus the co-occurrence matrix contains N^2 elements that can be considered as a reduced set of features. Some of the parameters that can be derived from the matrix can be given as follows, where μ_x, μ_y and σ_x, σ_y σ_x, σ_yas the mean and standard deviation derived from this matrix. The parameters are given as:

- *Angular second moment (energy)*: Energy also means uniformity, or angular second moment. The more homogeneous the image is, the larger the value. The image is believed to be a constant image when energy equals to 1.

$$\sum_{i=0}^{N-1}\sum_{j=0}^{N-1}[p(i,j)]^2 \tag{12}$$

- *Correlation:* This feature measures how correlated a pixel is to its neighbourhood. It is defined as,

$$\sum_{i=0}^{N-1}\sum_{j=0}^{N-1}\frac{ijp(i,j)-\mu_x\mu_y}{\sigma_x\sigma_y} \tag{13}$$

- *Inertia (Contrast):* Contrast measures the quantity of local changes in an image. It reflects the sensitivity of the textures in relation to changes in the intensity. It returns the measure of intensity contrast between a pixel and its neighbourhood.

$$\sum_{i=0}^{N-1}\sum_{j=0}^{N-1}(i-j)^2\,p(i,j) \tag{14}$$

- *Absolute value:* Measures the intensities of the image.

$$\sum_{i=0}^{N-1}\sum_{j=0}^{N-1}|i-j|p(i,j) \tag{15}$$

- *Inverse Difference*: Influenced by the homogeneity of the image. The result is a low inverse difference value for inhomogeneous images, and a relatively higher value for homogeneous images.

$$\sum_{i=0}^{N-1}\sum_{j=0}^{N-1}\frac{p(i,j)}{1+(i-j)^2} \tag{16}$$

- *Entropy*:: It denotes the randomness of intensity image.

$$H = -\sum_{i=0}^{N-1}\sum_{j=0}^{N-1}p(i,j)\log_2[p(i,j)] \tag{17}$$

Using above discussed parameters feature vector generates that can help in classification of the input image into the predetermined class label.

Volume 3, Issue 4; July-August 2020; Page No.372-389

Classification

Classification step occurs in two consecutive steps: learning phase and testing phase. The first one is known as training phase. It is the first step in classification. In this step it needs to build a model that can successfully classify a dataset. Back propagation algorithm is an optimization procedure based on gradient descent that adjusts the weights to reduce the system error. During the learning phase, input patterns are presented to the network and the network parameters are changed to bring the actual outputs closer to the desired target values. These outputs are compared to the target values. Any difference indicates an error. These errors are some scalar function of the weights. So the weights are to be adjusted for reducing the errors. This error function is the sum of square differences of the outputs and targets. Thus, the errors computed at the output layer are used to adjust the weights between the last hidden layer and the output layer.

The Artificial Neural Network System (ANFIS) uses fuzzy rules and fuzzy reasoning that is based on fuzzy set theory. It can also be said that fuzzy stands out to be a form of multi valued logic. FIS is based upon the concepts of fuzzy set theory, fuzzy if-then rules and fuzzy reasoning. In case of fuzzy if-then rules which take the following form:

$$if\ x\ is\ A\ then\ y\ is\ B \tag{18}$$

Here A and B are linguistic values which is defined by fuzzy sets on the universe of discourse of X and Y respectively. The statement "$x\ is\ A$" is called the antecedent and the statement "$y\ is\ B$" is called the consequence. The relation between two variables x and y in which the fuzzy rule defined as a binary relation R on the product space $X \times Y$. A fuzzy model can assume the following form of fuzzy rules:

$$if\ x\ is\ A\ and\ y\ is\ B\ then\ z = f(x, y) \tag{19}$$

Here A and B are fuzzy rules and $z = f(x,y)$ is a crisp on the input variables x and y. A two input ANFIS has been shown in Figure 2.

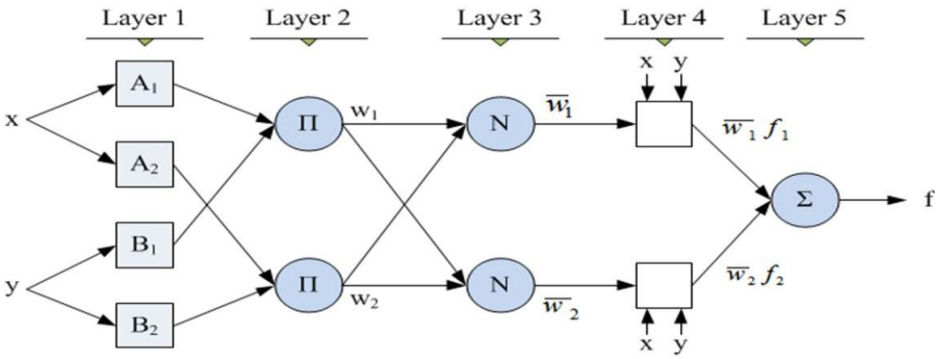

Figure 2: ANFIS architecture equivalent to fuzzy inference system

Each i[th] node in the a particular layer l takes an input from the previous layer and produces an output $O_{l,i}$. Now mapping for each individual layer is presented below:

- For layer 1 we take $l = 1$ and output as $O_{1,i}$ for each i[th] node in this layer. Every node in this layer is considered to be an adaptive node where the node function can be described as:

$$O_{1,i} = \begin{cases} \mu_{A_i}(x) & \text{for i} = 1,2 \\ \mu_{B_{i-2}}(y) & \text{for i} = 3,4 \end{cases} \tag{20}$$

Here x or y is the input variable to node i and each node is assigned a linguistic label A_i or B_{i-2} to it. Here $\mu_A(x)$ denotes the membership function for A and can be any

Volume 3, Issue 4; July-August 2020; Page No.372-389

valid parameterized function that depends on a parameter set. This parameter set can also be called as premise parameters.

- In the next layer (Layer 2) we consider a fixed node label denoted by Π for which the output for the incoming signal can be defined by:

$$O_{2,i} = w_i = \mu_{A_i}(x)\mu_{B_i}(y) \qquad \text{for i} = 1,2$$

(.21)

This output represents the firing strength of a rule.

- layer 3 calculate the normalized firing strengths for every i^{th} node and can be calculated as the ratio between the firing strength of that layer to the sum of all firing rules in that layer as:

$$O_{3,i} = \overline{w_i} = \frac{w_i}{\sum_{i=1}^{2} w_i}$$

(22)

- In layer 4 computes the output considering the parameter set embedded in the membership function. The parameters in this set are referred as consequent parameters. The node function for every i^{th} node can be given as:

$$O_{4,i} = \overline{w_i} f_i(x, y)$$

(23)

- In the last layer (layer 5) each of the node is assigned with a fixed node label Σ. Each node computes the summation of all incoming signals as outputs as:

$$O_{5,i} = \sum_i \overline{w_i} f_i(x, y) = \frac{\sum_i w_i f_i(x, y)}{\sum_i w_i}$$

(24)

In this model it has been observes that if a particular tuple does not match with the established fuzzy rules defined in the model, the classifier tries to give a result that is outside the solution set. This is helpful in determining a new type of tumour.

Results and Analysis

The images are normalized to the feature vector containing 12 features are extracted from the slices. Each of the feature vector forms an input tuple to the classifier. This vector is generated for 20 input slices shown in Figure 3 has been illustrated by Table 1 and Table 2.

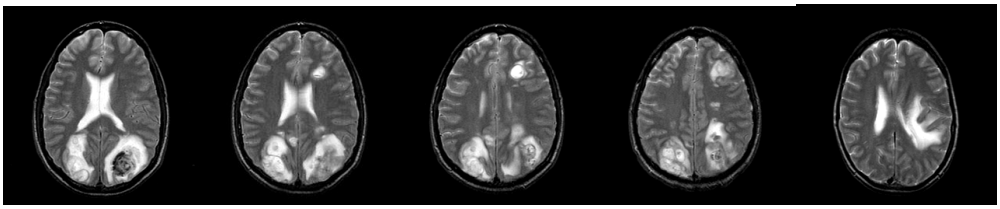

(I1) (I2) (I3) (I4) (I5)

Volume 3, Issue 4; July-August 2020; Page No.372-389

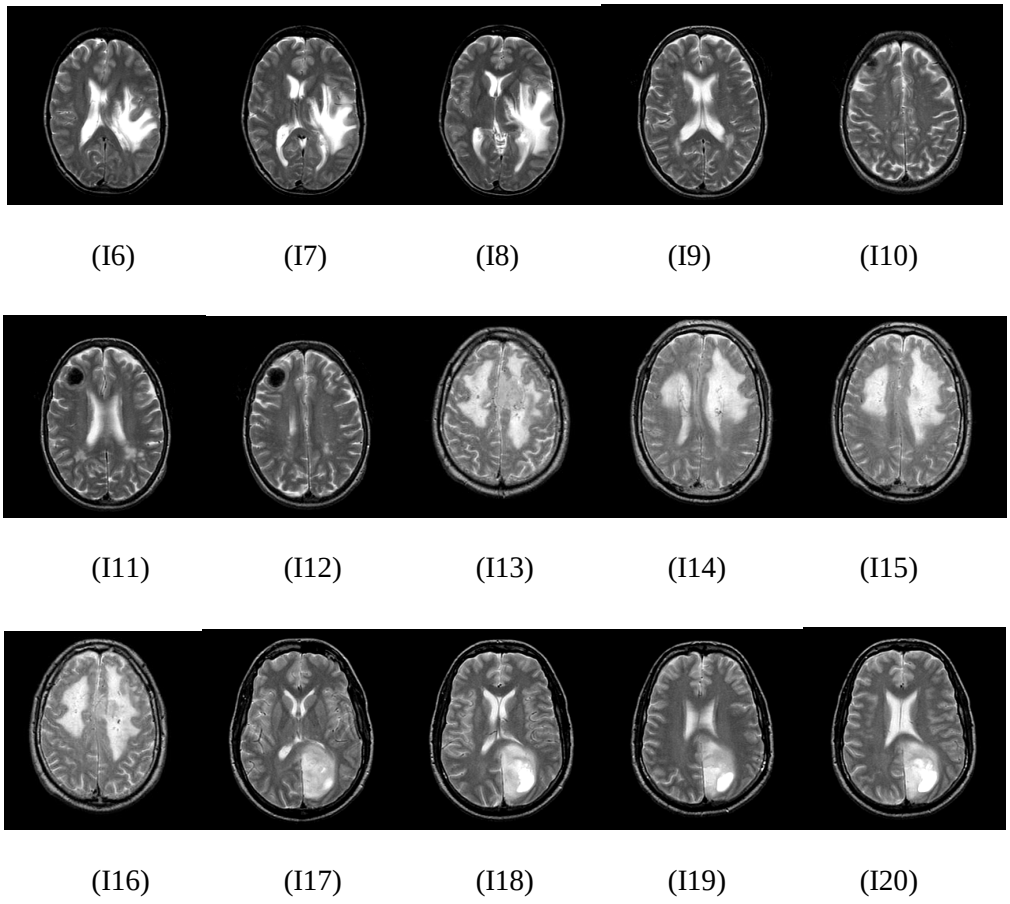

Figure 3: 20 input slices passed through the normalization and feature extraction processes for classification. After classification it is found that slices I1-I4 are Type 1 (Sarcoma); slicesI5-I8 are Type 2 (Meningioma); slices I9-I12 are Type 3 (Metastatic adenocarcinoma); slices I13-I16 are Type 4 (Metastatic bronchogenic carcinoma);slicesI17-I20 are Type 5 (Glioma)

Each of the generated feature vector from the normalized grayscale image are calculated from 1st order histogram based features and features from Gray Level Co-occurrence Matrix. Each of the functions derives a single valued element in the feature extraction matrix for each of the 20 slices that is represented in Table 1 and Table 2.

Table 1: Feature vector from the normalized grayscale MR image

Image sequence	Mean	Variance	Skewness	Kurtosis	Energy	Entropy
1	15.5399	446.433	0.000108	0.000127	0.2816	3.6817
2	14.7607	427.681	0.000126	0.000151	0.2933	3.5751

Volume 3, Issue 4; July-August 2020; Page No.372-389

3	15.5426	447.411	0.000108	0.000127	0.2810	3.6939
4	15.3294	434.847	0.000116	0.00014	0.2762	3.7014
5	15.9980	466.920	0.0001	0.000118	0.2718	3.8210
6	16.2995	455.317	0.000972	0.000117	0.2540	3.8918
7	16.8535	461.050	0.000906	0.00011	0.2365	3.9722
8	15.2010	463.274	0.000113	0.000132	0.2981	3.6796
9	13.6257	406.182	0.00015	0.000185	0.3333	3.2856
10	13.9531	413.331	0.000143	0.000175	0.3219	3.4029
11	13.1538	400.748	0.000161	0.000200	0.3529	3.2298
12	14.2234	417.177	0.000137	0.000165	0.3123	3.4526
13	13.6782	420.489	0.000142	0.000167	0.3506	3.2687
14	13.5103	417.582	0.000144	0.000169	0.3583	3.1849
15	13.2064	412.893	0.000151	0.000178	0.3698	3.1134
16	12.3658	388.257	0.000181	0.000226	0.3857	3.0153
17	12.9241	397.207	0.000167	0.00021	0.3573	3.2094
18	13.5875	407.496	0.000151	0.000185	0.3342	3.3352
19	14.2193	425.415	0.000137	0.000164	0.3174	3.4692
20	14.9834	443.361	0.000118	0.000138	0.3040	3.5664

Table 2: Feature vector of normalized grayscale MR image

Image sequence	Contrast	Correlation	Energy	Homogeneity	Inverse difference	Absolute value
1	0.3334	0.3878	0.4131	0.8726	56710.6	17910
2	0.3190	0.3833	0.4379	0.8774	57036.6	17210
3	0.3415	0.3862	0.4071	0.8697	56512.8	18328
4	0.3547	0.3508	0.4112	0.8659	56247.2	18914
5	0.3618	0.3884	0.3971	0.8663	56246	18994

Volume 3, Issue 4; July-August 2020; Page No.372-389

6	0.3499	0.3785	0.3871	0.8652	56218.6	18910
7	0.3697	0.3640	0.3731	0.8592	55806.6	19812
8	0.3610	0.3920	0.4227	0.8712	56534.6	18504
9	0.2931	0.3803	0.4756	0.8861	57632.2	15936
10	0.2984	0.3755	0.4668	0.8831	57439.6	16314
11	0.2885	0.3749	0.4930	0.8896	57854	15516
12	0.3019	0.3595	0.4589	0.8800	57245.4	16676
13	0.2558	0.4260	0.4907	0.8970	58395.4	14258
14	0.2565	0.4179	0.4908	0.8972	58406	14248
15	0.2443	0.4349	0.5019	0.9011	58674.6	13668
16	0.2395	0.4074	0.5274	0.9029	58796.6	13412
17	0.2881	0.3883	0.4918	0.8902	57893.2	15446
18	0.2936	0.3933	0.4727	0.8867	57670.4	15878
19	0.3158	0.3685	0.4617	0.8804	57227	16858
20	0.3164	0.3804	0.4429	0.8786	57115.6	17050

Each tuple contains its class label which denotes its tumour type which is used to build IF-THEN rules to generate the FIS. ANFIS is trained network that is used to generate the class label for the input slices. The class labels mentioned here were taken accordingly as: Class 1 = Sarcoma, Class 2 = Meningioma, Class 3 = Metastatic adenocarcinoma, Class 4 = Metastatic bronchogenic carcinoma, Class 5 = Glioma. The classifier gives fuzzy numbers as output which is de-fuzzified to get the crisp actual class labelled values.

Performance measurement

Performance is measured by comparing the actual class labels and the predicted class labels for each of the individual classifiers. In statistical analysis of classification, the F-score or F-measure is a measure of a test's accuracy. Performance measurement metrics value of 5 major tumour types as different class has been shown in Table 3.

Table 3: Performance measurement metrics value of 5 major tumour types

Metric	**Class 1**	**Class 2**	**Class 3**	**Class 4**	**Class 5**
True Positive (TP)	37	43	32	29	48
False Negative (FN)	4	4	5	2	4

Volume 3, Issue 4; July-August 2020; Page No.372-389

False Positive (FP)	3	3	2	6	5
True Negative (TN)	164	158	169	171	151
Sensitivity(TP/(TP+FN))	0.902	0.914	0.864	0.935	0.923
Specificity(TN/(FP+TN))	0.982	0.981	0.988	0.966	0.967
Precision(TP/(TP+FP))	0.925	0.934	0.941	0.828	0.905
Accuracy((TP+TN)/(P+N))	0.966	0.966	0.966	0.961	0.956
F score(2TP/(2P+FP+FN))	0.913	0.924	0.901	0.878	0.914

The performance of the classifiers is evaluated in terms of sensitivity, specificity, precision, accuracy and F score. The average value of sensitivity is 0.90815166, average value of specificity is 0.977151379, average value of precision is 0.907038177, average value of accuracy is 0.963461538, and average value of F score is 0.906558695 for an ANFIS. ROC curve of proposed system has been shown in Figure 4.

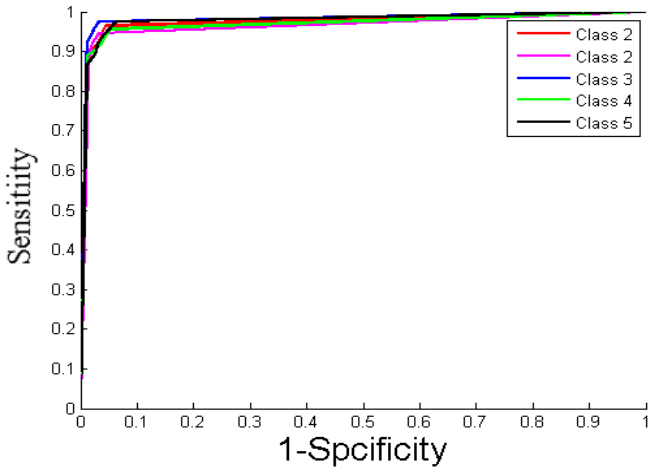

Figure 4: ROC curve for brain tumour classification

The proposed method, as discussed above, applied now for the entire data set before COVID-19 and during COVID-19. Initially dataset of five months of MRIs of patients along with their diagnosis by radiologists are shown in table 4- table 8. The graphical representations of diagnosis of patients for each month are given after each table in the form of figure 5 to figure 9. Table 10 shows total collected MRIs. Figure 11 indicates graphical representation of collected data. The performance measure metrics such as Accuracy, F1-score, and Cohen-Kappa score are used for evaluating the prediction. Table 12 shows performance measure of patients before and after COVID-19. method. Figure 13 to figure 15 show the measures of Accuracy, F1-score, and Cohen-Kappa score.

Volume 3, Issue 4; July-August 2020; Page No.372-389

Days	Total)MRI)Reports)Collected)for patients)came)for)testing)brain)problem	Normal	Sign)of)Tumour	Abnormality)Detected
5	500	485	13	2
9	180	170	6	4
16	450	425	20	5
20	300	280	17	3
22	900	850	40	10
25	250	200	30	20
27	57	45	10	2
30	78	60	14	4
Total	2715	2515	150	50

Table 4 January 2020: Total MRIs and their Statistics

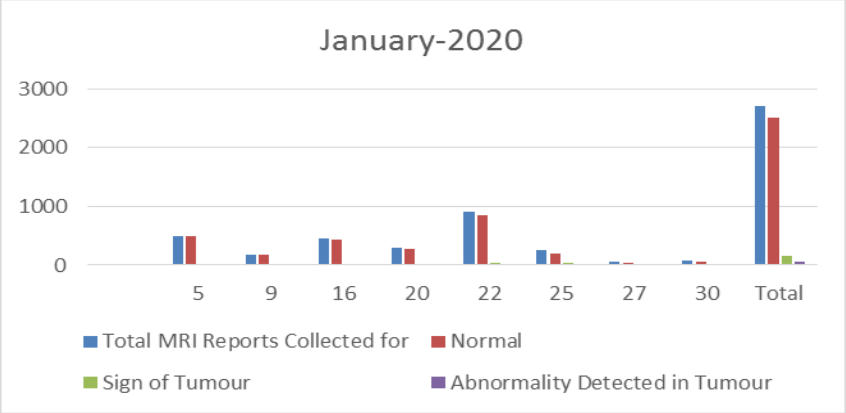

Figure 5 Jan-2020: It shows MRIs of Normal, Sign of Tumour and Abnormality Detected

Days	Total)MRI)Reports)Collected)for patients)came)for)testing)brain)problem	Normal	Sign)of)Tumour	Abnormality)Detected
5	1500	1400	180	20
9	900	970	25	5
16	450	425	20	5
20	300	280	17	3
22	1200	1100	60	40
25	250	200	30	20
27	57	45	10	2
30	78	60	14	4
Total	4735	4480	356	99

Table 5 February 2020: Total MRIs and their Statistics

Volume 3, Issue 4; July-August 2020; Page No.372-389

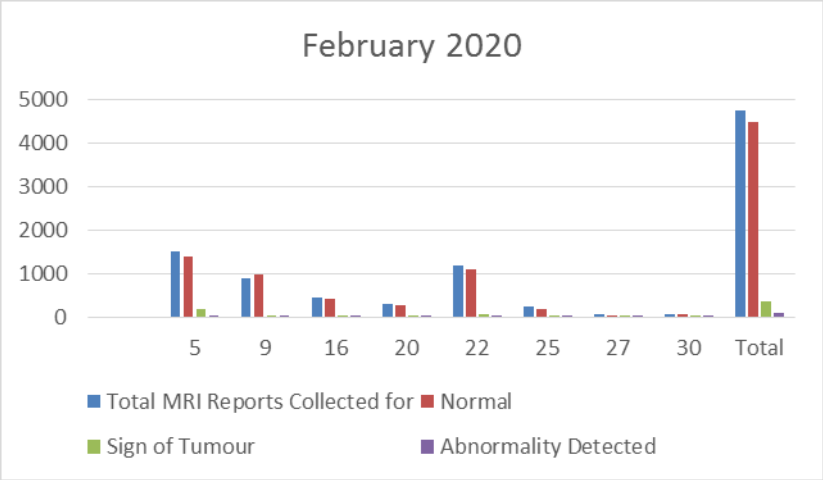

Figure 6 February-2020: It shows MRIs of Normal, Sign of Tumour and Abnormality Detected

Days	Total)MRI)Reports)Collected)for patients)came)for)testing)brain)problem	Normal	Sign)of)Tumour	Abnormality)Detected
5	500	400	56	44
9	2000	1800	150	50
16	450	425	20	5
20	300	280	17	3
22	1200	1100	60	40
25	250	200	30	20
27	300	225	45	30
30	78	60	14	4
Total	5078	4490	392	196

Table 6 April 2020: Total MRIs and their Statistics

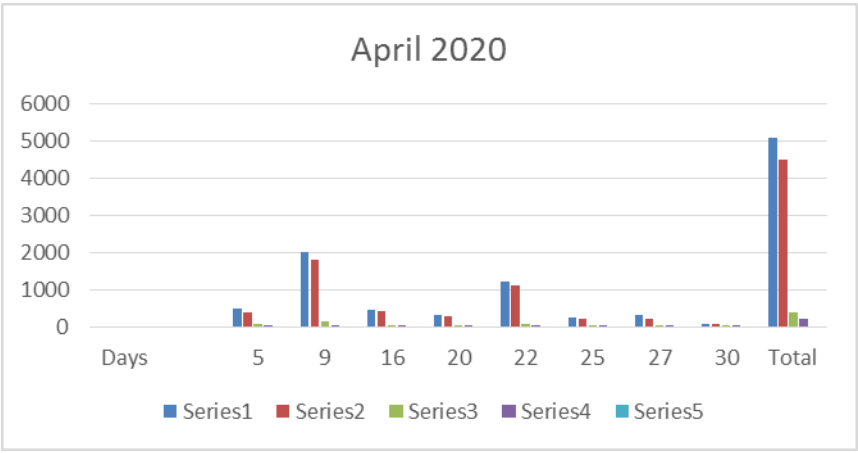

Figure 7 April-2020: It shows MRIs of Normal, Sign of Tumour and Abnormality Detected

Volume 3, Issue 4; July-August 2020; Page No.372-389

Days	Total)MRI)Reports)Collected)for patients)came)for)testing)brain)problem	Normal	Sign)of)Tumour	Abnormality)Detected
5	400	300	40	60
9	2000	1800	150	50
16	1600	1500	55	45
20	1300	1200	70	30
22	1200	1100	60	40
25	250	200	30	20
27	800	680	100	20
30	900	800	40	60
Total	8450	7580	545	325

Table 7 May 2020: Total MRIs and their Statistics

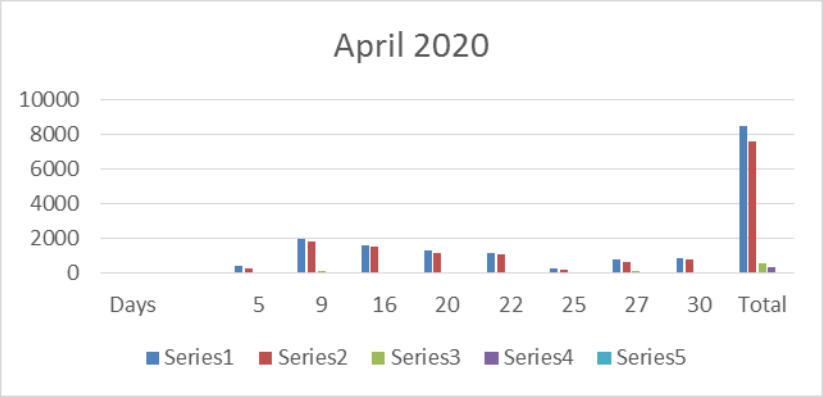

Figure 8 May-2020: It shows MRIs of Normal, Sign of Tumour and Abnormality Detected

Days	Total)MRI)Reports)Collected)for patients)came)for)testing)brain)problem	Normal	Sign)of)Tumour	Abnormality)Detected
5	1400	1200	150	50
9	2000	1800	130	70
16	1500	1400	20	80
20	1300	1200	70	30
22	1200	1100	60	40
25	600	400	120	80
27	800	680	100	20
30	900	800	40	60
Total	9700	8580	690	430

Table 8 June 2020: Total MRIs and their Statistics

Volume 3, Issue 4; July-August 2020; Page No.372-389

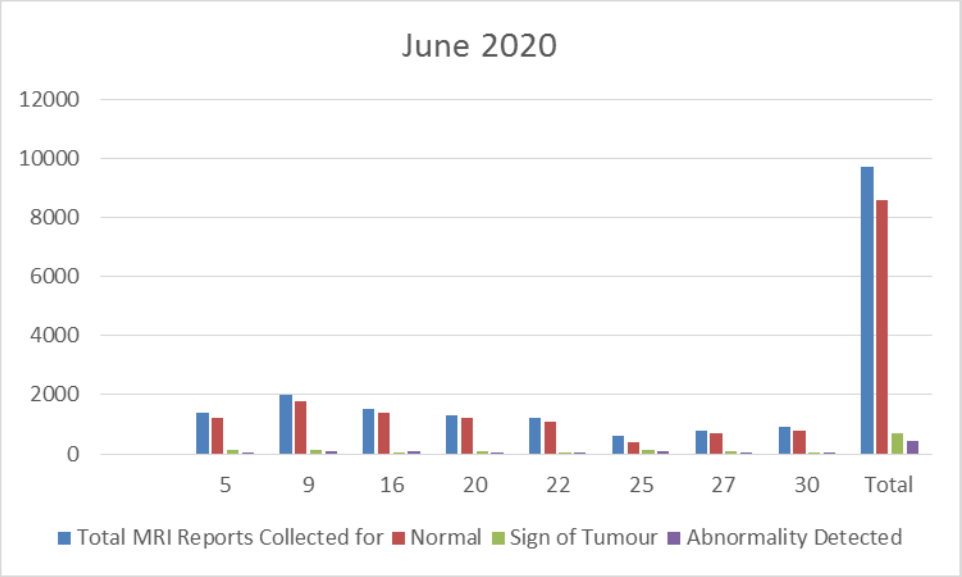

Figure 9 June-2020: It shows MRIs of Normal, Sign of Tumour and Abnormality Detected

Month	
January	2715
February	4735
April	5078
May	8450
June	9700
Total	30678

Table 10 Total collected MRIs

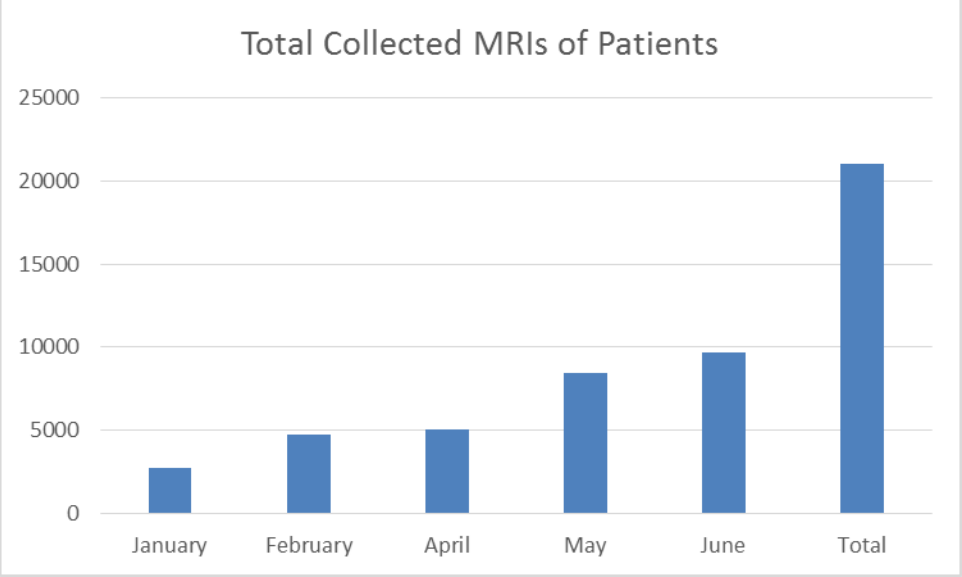

Figure 11: Graphical representation of collected data

Volume 3, Issue 4; July-August 2020; Page No.372-389

Month	Accuracy	F1-Score	Cohen-Kappa Score
January	92%	0.89	0,21
February	93%	0.88	0.29
April	91%	0.91	0.35
May	95%	0.93	0.38
June	96%	0.94	0.35

Table 12 Performance measure of patients before and after COVID-19

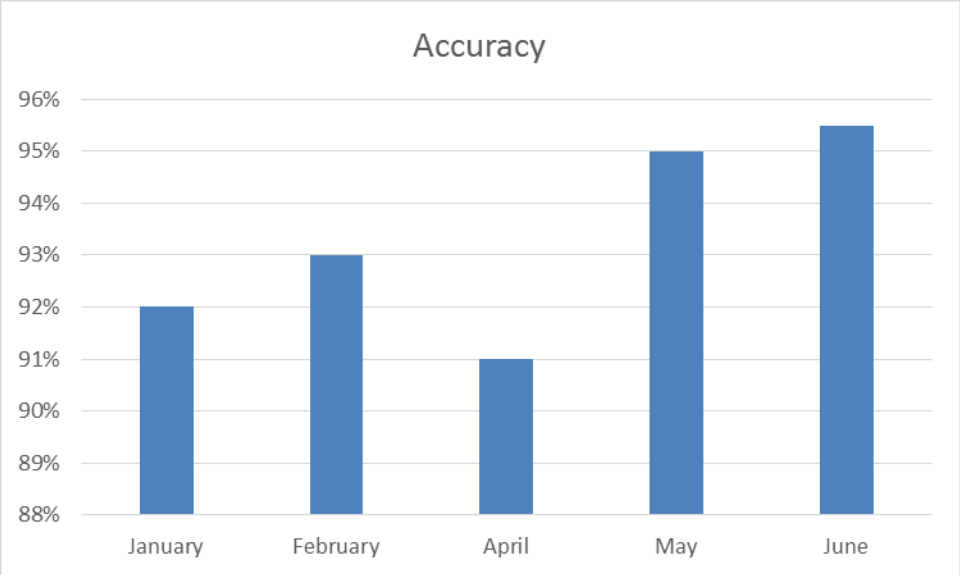

Figure 13 Accuracy measure before and after COVID-19

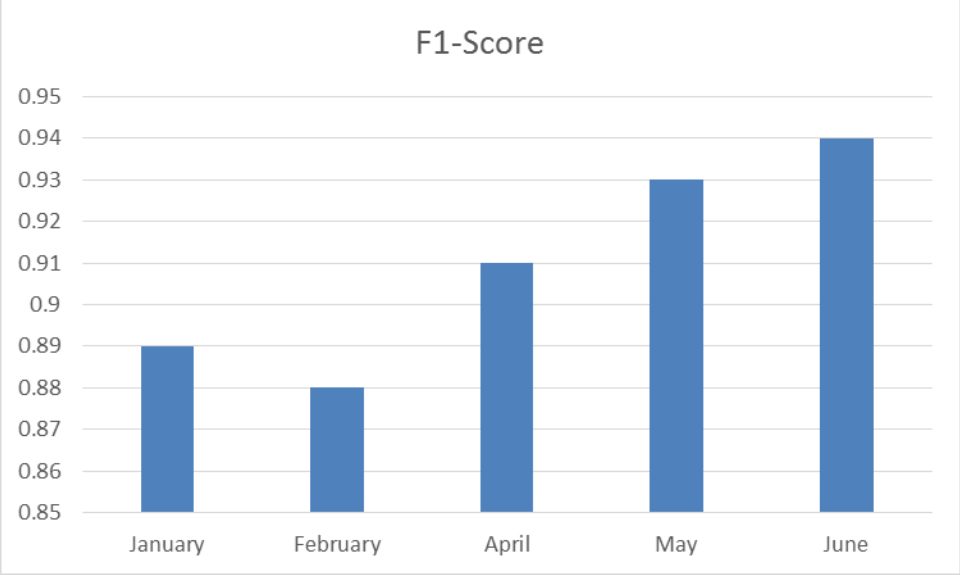

Figure 14 F1-score before and after COVID-19

Cohen-Kappa Score

Volume 3, Issue 4; July-August 2020; Page No.372-389

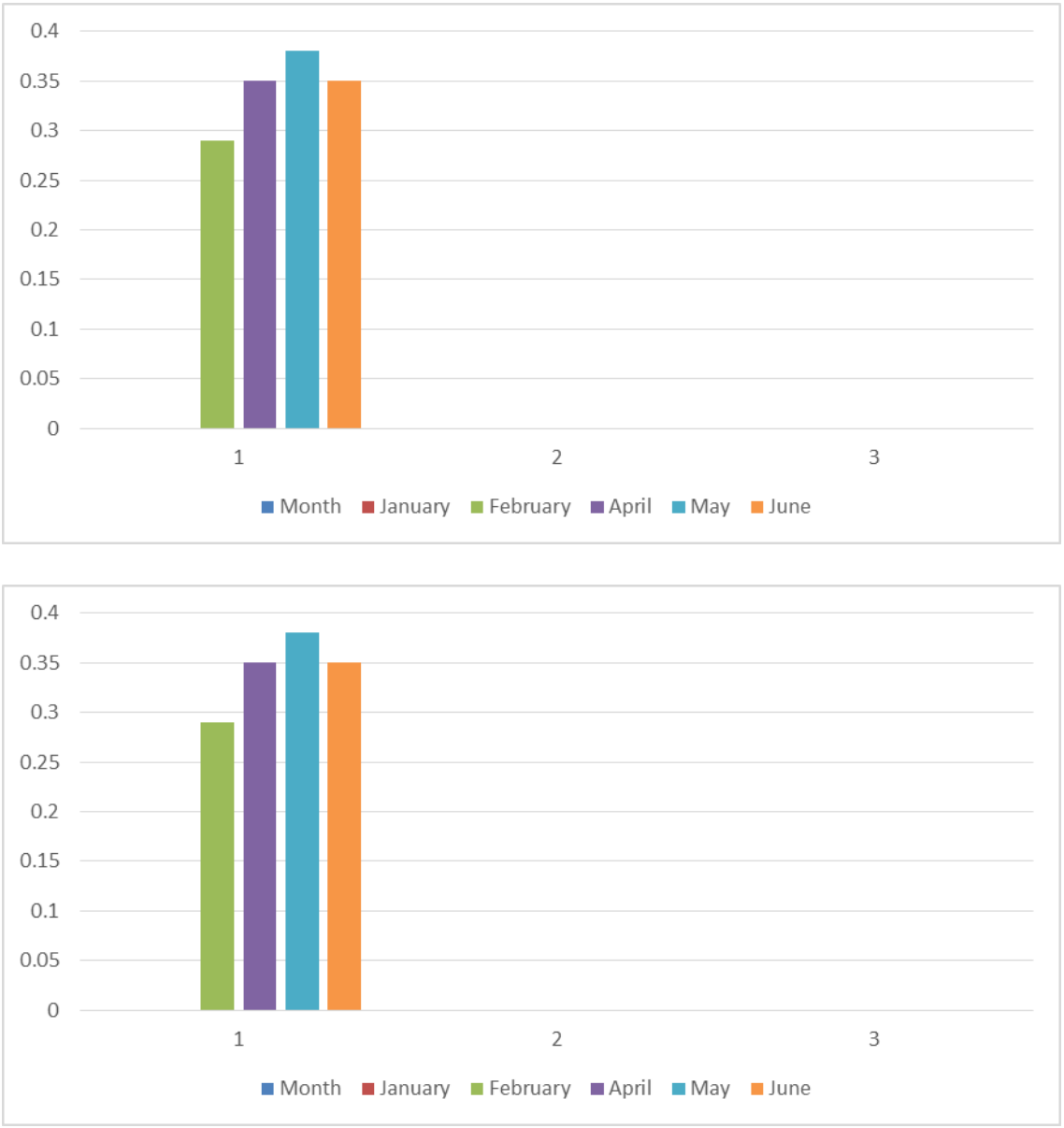

Figure 15 Cohen-Kappa Score before and after COVID-19

Conclusions

The datasets are collected from various hospitals in West Bengal. The results obtained by the proposed approach indicate that there is a variations of sign of abnormalities before and after COVID-19. It also correctly detected the abnormalities, if present. The performance measures such as Accuracy, F1-score and Cohen-Kappa score are calculated for five months and graphically presented in the result section.

References

1. E. E. M. Azhari, M. M. M. Hatta, Z. Z. Htike, and S. L. Win, "Tumor detection in medical imaging: a survey," International Journal of Advanced Information Technology, 2014.
2. J. Liu, M. Li, J. Wang, F. Wu, T. Liu, and Y. Pan, "A survey of MRI based brain tumor segmentation methods," Tsinghua Science and Technology, 2014.
3. S. Shen, W. Sandham, M. Granat, and A. Sterr, "MRI fuzzy segmentation of brain tissue using neighborhood attraction with neural-network optimization," IEEE Transaction on Information Technology in Biomedicine, 2005.

Volume 3, Issue 4; July-August 2020; Page No.372-389

4. D. L. Pham, C. Xu, and J. L. Princem, "Current methods in medical image segmentation," Annual Review of Biomedical Engineering, 2000.
5. T. Logeswari and M. Karnan, "An improved implementation of brain tumor detection using segmentation based on hierarchical self-organizing map," International Journal of Computer Theory and Engineering, 2010.
6. N. B. Bahadure, A. K. Ray, and H. P. ethi, "Image analysis for MRI based brain tumor detection and feature extraction using biologically inspired BWT and SVM," International Journal of Biomedical Imaging, 2017.
7. A. Hanuman and K. Sooknanan, "Brain tumor segmentation and volume estimation from T1-contrasted and T2 MRIs," International Journal of Image Processing (IJIP), 2018.
8. A. Hazra, A. Dey, and S. K. Gupta, M. A. Ansari, "Brain tumor detection based on segmentation using MATLAB," in Proceedings of the International Conference on Energy, Communication, Data Analytics and So- Computing (ICECDS), IEEE, Piscataway, NJ, USA, 2017.
9. A. Gujar and C. M. Meshram, "Brain tumor extraction using genetic algorithm," International Journal on Future Revolution in Computer Science and Communication Engineering (IJFRSCE), 2018.
10. S. Pereira, A. Pinto, V. Alves, and C. A. Silva, "Brain tumor segmentation using convolutional neural networks in MRI images," IEEE Transactions on Medical Imaging, 2016.
11. I. Kullayamma and A. Praveen Kumar, "Brain tumor segmentation by using ant colony optimization," International Journal of Scientific Research in Science and Technology, 2018.
12. Lian W, Guan W, Chen R et al. Cancer patients in SARS-CoV-2 infection: a nationwide analysis in China. Lancet Oncol., 2020;
13. COVID-19 Map—Johns Hopkins Coronavirus Resource Center. https:// coronavirus.jhu.edu/map.html. ,April 2020.
14. Hanna TP, Evans GA, Booth CM. Cancer, COVID-19 and the precautionary principle: prioritizing treatment during a global pandemic. Nat Rev ClinOncol, 2020..
15. Wu X, Nethery RC, Ma MBS, Braun D. Exposure to air pollution and COVID-19 mortality in the United States: medRxiv, 2020.
16. Mahase E. Covid-19: use radiotherapy only if 'unavoidable', says NICE. BMJ. April 2020.

Volume 3, Issue 4; July-August 2020; Page No.372-389